OPTICA

Control of intense light with avalanche-ionization plasma gratings

M. R. Edwards,[1,2,*] S. Waczynski,[3] E. Rockafellow,[3] L. Manzo,[1] A. Zingale,[3] P. Michel,[1] and H. M. Milchberg[3]

[1]Lawrence Livermore National Laboratory, Livermore, California 94551, USA
[2]Stanford University, Stanford, California 94305, USA
[3]Institute for Research in Electronics and Applied Physics, University of Maryland, College Park, Maryland 20742, USA
*mredwards@stanford.edu

Received 16 August 2023; revised 17 October 2023; accepted 18 October 2023; published 21 November 2023

High-peak-power lasers are fundamental to high-field science: increased laser intensity has enabled laboratory astrophysics, relativistic plasma physics, and compact laser-based particle accelerators. However, the meter-scale optics required for multi-petawatt lasers to avoid light-induced damage make further increases in power challenging. Plasma tolerates orders-of-magnitude higher light flux than glass, but previous efforts to miniaturize lasers by constructing plasma analogs for conventional optics were limited by low efficiency and poor optical quality. We describe a new approach to plasma optics based on avalanche ionization of atomic clusters that produces plasma volume transmission gratings with dramatically increased diffraction efficiency. We measure an average efficiency of up to 36% and a single-shot efficiency of up to 60%, which is comparable to key components of high-power laser beamlines, while maintaining high spatial quality and focusability. These results suggest that plasma diffraction gratings may be a viable component of future lasers with peak power beyond 10 PW.

https://doi.org/10.1364/OPTICA.503283

1. INTRODUCTION

Extreme light intensities [1]—above 10^{20} W/cm^2—are critical for studying relativistic optics [2], accelerating electrons and ions [3–5], performing scaled laboratory astrophysics experiments [6], and probing quantum electrodynamics [7]. The only tool currently capable of producing fields of these strengths is the high-peak-power laser [8], which has grown remarkably in capability since the invention of chirped pulse amplification (CPA) [9]. However, at 1–10 PW peak powers, these femtosecond-pulse-duration lasers require meter-diameter mirrors and gratings to keep the intensity of light within the system below the terawatt/cm^2 optical damage thresholds of solid materials. The costs associated with optics of this size have slowed the development of higher-power lasers. Reaching higher light intensity, which is necessary for more robust high-intensity interactions and for probing Schwinger-limit physics in the laboratory frame [10,11], requires either prohibitively expensive lasers (10 m or larger beam diameters) or a fundamentally new approach to controlling intense light.

High-intensity light turns all materials to plasma, so it is natural to ask whether intensity-resistant optics can be built with plasma: creating a *plasma optic* [12]. The limits on light intensity for a plasma optic are set by plasma nonlinearities or relativistic effects, allowing intensities 2 to 5 orders of magnitude higher than what would damage a solid-state optic [13]. This unique robustness of plasma to optical damage has driven research on a variety of plasma optics based on either the linear index of refraction of a plasma or nonlinear wave-mixing processes, including amplifiers [14–21], waveplates [22–24], lenses [25–27], waveguides [28,29], mirrors [30–33], and gratings [34–36]. Although theory and simulations suggest plasma optics are capable of performance similar to their solid-state counterparts, optical-quality plasmas have proven difficult to create and—with the exception of plasma mirrors, which have limited applications—experimentally demonstrated plasma optics are poor quality and inefficient. To be useful, a plasma grating must be scalable to high energy and achieve a diffraction efficiency comparable to other components of high-power beamlines, e.g., grating compressors (75%) [37] or double plasma mirrors (60%) [38–40]. Thus far, it is unclear that any plasma optic apart from a plasma mirror can reach this regime.

A volume transmission grating may be more robust than other types of optics to the plasma imhomogeneities and imperfections that have hindered previous experiments [13]. Transmission gratings are broadly useful for designing high-power laser systems, allowing redirection, controllable dispersion, and focusing [26,27] of high-intensity light pulses; an efficient plasma transmission grating is the only plasma optic required to significantly improve the capability of high-power lasers [13]. Plasma transmission gratings are based on inducing a refractive index modulation, i.e., a density modulation, in a plasma and can be constructed using ionization [34,41–47] or the ponderomotive force [35,36,48–50], which drives charged particles away from regions of high light intensity.

Ionization gratings are formed when the intensity interference pattern of two equal-wavelength laser pulses crossed in a medium produces periodic layers of ionized (plasma) and neutral material [34,42,46]. The resultant structure has a spatially modulated refractive index and for a subsequent probe pulse acts as a volume diffraction grating. Ionization gratings are more readily created in the laboratory than ponderomotively driven gratings, so in the near-term they are a more useful experimental platform for exploring the possibilities and limits of plasma gratings.

Over the last decade, ionization gratings have been produced by the field ionization of air [34,42] and uniform gas [46] by millijoule-energy femtosecond pulses. This configuration is simple, but the grating shape is determine solely by the overlap geometry, fundamentally restricting both efficiency and optical quality [51]. The highest previously demonstrated efficiency from an ionization grating is less than 19% [42]. Furthermore, filamentation [52] of the pumps during extended high-intensity propagation in air constrains the grating size. Although volume ionization gratings are among the most promising and potentially useful plasma optics, these previous efficiency and optical quality results are far from the >50% efficiencies required for high-power beamline components.

Here, we demonstrate for the first time that it is possible to reach useful diffraction efficiency with an ionization grating, showing up to 60% of incident light redirected into a diffracted beam. This result comes from a new approach based on collisional (avalanche) ionization gratings driven by picosecond pump pulses in gas and cluster jets. Collisional ionization is the process by which free electrons accelerated by a laser field acquire sufficient energy to free further electrons during collisions with neutral species; significant plasma densities can be achieved at a lower pump laser intensity than that required by field ionization [53]. By lowering the required pump intensity, this approach reduces pump filamentation and other nonlinear limits. Although the highest efficiencies we observe (50%–60%) were found only in individual single-shot measurements, we also achieved an average efficiency of up to 36%, double previous records. Additionally, we have made the first measurements of the stability and focusability of a beam diffracted from an ionization grating, showing that high-spatial-quality diffraction is possible. We present here measurements of the grating dynamics, together with characterization of diffraction efficiency, spatial quality, and performance at intensities up to 10^{14} W/cm^2. This grating is not yet suitable for slotting into a high-power laser system, but we have found that there is no fundamental limit preventing plasma gratings with useful efficiencies. This suggests that continued development of plasma gratings could lead to viable optical elements for high-power laser systems.

2. RESULTS

A. Grating Design and Formation

The intensity interference pattern produced by two pump laser beams with wavelength λ_0 and crossing half-angle θ_0 is a one-dimensional oscillation with period $\Lambda = \lambda_0/(2n_0 \sin\theta_0)$, where n_0 is the average refractive index, as drawn in Fig. 1(a). If the pump beam overlap occurs in a finite medium (in z) and the peak intensity is sufficient for ionization, this will produce a spatially modulated distribution of free electrons (density N_e) with period Λ and thickness D. The refractive index (n) of a plasma depends on electron density [$n = \sqrt{1 - N_e/N_c}$, where $N_c = \varepsilon_0 m_e (2\pi c)^2/(e^2\lambda_1^2)$ is the critical density for wavelength λ_1, ε_0 is the vacuum permittivity, m_e and e are the electron mass and charge, and c is the speed of light], so a modulated plasma density corresponds to a spatially varying refractive index, $n(x) = n_0 + \delta n(x)$, where if $n(x)$ is expressed as a sum of Fourier modes, n_1 is the coefficient of the mode with period Λ [54]. This distribution of n acts as a volume diffraction grating with a Bragg angle (θ_B) for a subsequent probe laser given by $\sin\theta_B = \lambda_1/(2n_0\Lambda)$.

Although light propagation through volume gratings of arbitrary geometry is complicated, for a plane wave and an infinite-width (in x) grating the problem simplifies to two cases that can be analytically tackled with coupled mode theory [54]: reflection gratings, where the diffracted beam leaves the grating through the same surface that it entered, and transmission gratings, where the diffracted and undiffracted beams leave through the opposite surface. Both reflection and transmission gratings will diffract a probe, but they differ in the resultant diffraction angle (θ_2) of a beam incident at θ_1, with $\theta_2 = -\theta_1$ for a reflection grating and $\sin\theta_2 = \sin\theta_1 \pm \lambda_1/(n_0\Lambda)$ for a transmission grating [54]; volume transmission gratings are angularly dispersive. The diffraction efficiency (η_1), defined as the ratio of diffracted energy to incident energy, also differs. For a probe incident at the Bragg angle ($\theta_1 = \theta_B$), we have $\eta_1 = \tanh^2 \kappa D$ for reflection gratings and

$$\eta_1 = \sin^2 \kappa D \tag{1}$$

for transmission gratings, where D is the grating thickness and the coupling constant $\kappa = \pi n_1/(\lambda_1 \cos\theta_B)$ [54,55]. For $\eta_1 \ll 1$, both simplify to $\eta_1 \approx (\kappa D)^2$. The envelope shape of gratings created via ionization in uniform gas is the overlap of the two pump beams and cannot be well approximated by the infinite-width condition; in this case, efficiency needs to be evaluated numerically. Since previous work on ionization gratings was at low efficiency ($\eta_1 < 0.2$, $\eta_0 \approx 1$, where η_0 is the undiffracted fraction of the incident energy), the small-η_1 limit has been adequate. However, in the depletion regime ($\eta_0 \ll 1$, $\eta_1 > \eta_0$), which is crucial for applications and which we enter here, the distinction between transmission, reflection, and non-ideal gratings substantially affects diffraction.

Transmission gratings are the critical ionization optic to demonstrate: they form the basis of diffractive plasma lenses [27] and dispersive plasma compressors [13] and have lower density and quality requirements than reflection gratings. For high-efficiency diffraction ($\eta_1 \approx 1$), a transmission grating must satisfy $2n_1 \approx \lambda_1 \cos\theta_B/D$, where n_1 depends on both the plasma density modulation and probe wavelength. Usefully for gratings where κ is not uniform, κD generalizes to the grating integral $\int_0^D \kappa(z)\mathrm{d}z$ [54], which is essential because gas jets and other methods for producing a finite medium create substantial plasma density gradients at their edges. Note that, in the Bragg regime, only n_1 should be considered when calculating the diffraction efficiency, not the total modulation Δn; a probe beam incident at the Bragg angle will be outside the acceptance angle of the other Fourier modes [54]. Figure 1(b) shows the efficiency calculated from Eq. (1) for $D = 1$ mm at both $\lambda_1 = 800$ nm and 3.9 μm. The inset illustrates different properties of the plasma electron density: the maximum density $N_e^{\max}$ is limited by the initial gas density; an interferometric measurement that does not resolve the fringes will return the average density ($N_{e,0}$); the total fluctuation ΔN_e may be limited by the

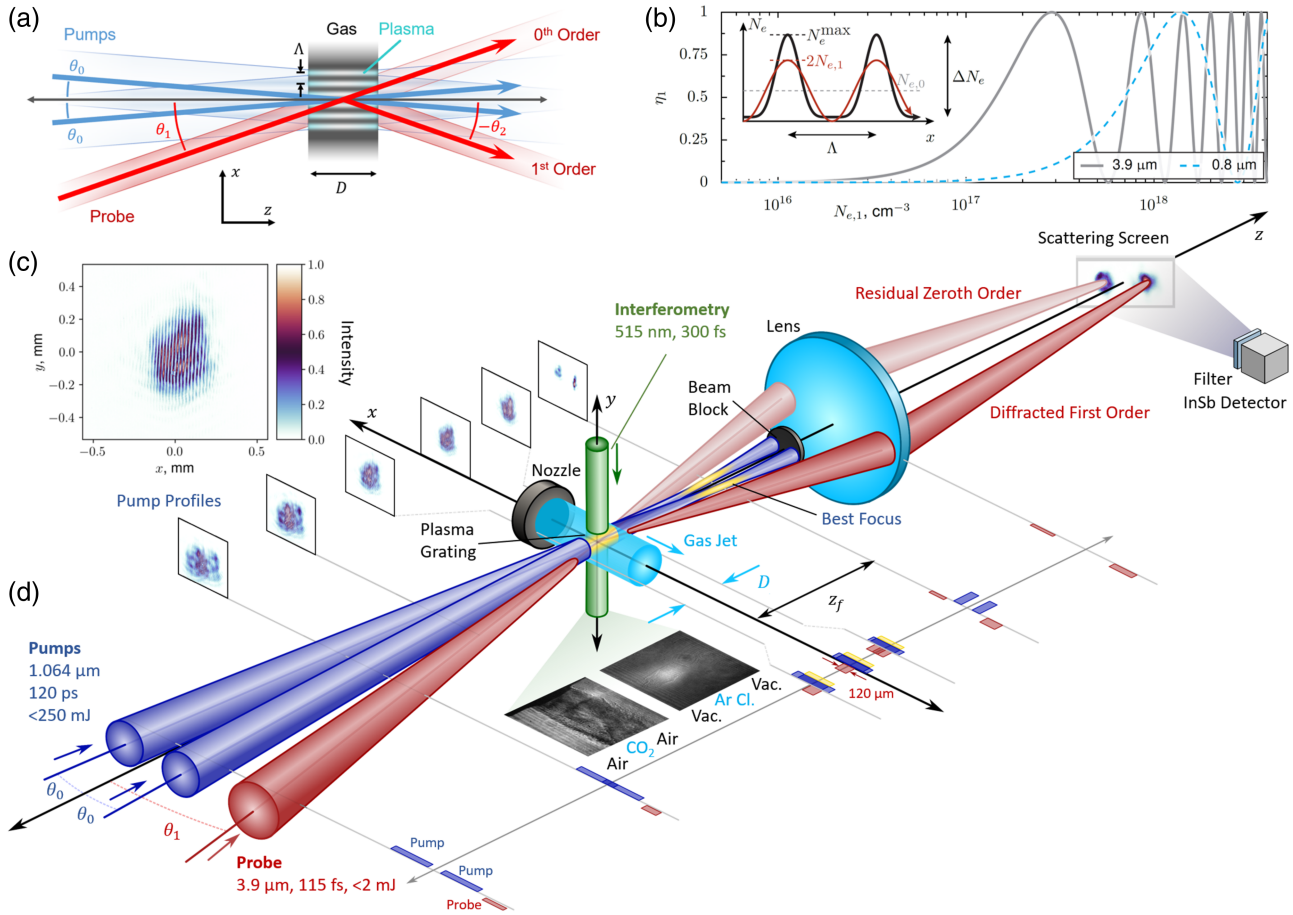

Fig. 1. Schematic of experiment and characterization of plasma. (a) Geometry of volume transmission grating induced by two pump lasers beams in a gas jet. (b) Analytic calculation of diffraction efficiency for $\lambda_1 = 3.9$ μm and 0.8 μm probes for $D = 1$ mm and varied grating density. Inset, schematic of relationship between different density quantities. (c) Intensity profile of the two pumps in the CO_2 jet configuration, measured at low power. (d) Layout of experiment, showing the two pump lasers driving a plasma grating in either a CO_2 or an argon cluster jet. A fraction of the delayed probe diffracts from the jet, and both the diffracted and undiffracted beams are imaged on a scattering screen.

pump interference contrast; and $N_{e,1}$, the amplitude of the sinusoidal component of the density, governs diffraction. If $N_e \ll N_c$ everywhere, each of these measures of density directly relates to the corresponding measure of refractive index, e.g., $n_1 \approx N_{e,1}/2N_c$.

We created high-efficiency ionization gratings using an optical parametric chirped pulse amplification (OPCPA) system providing a 3.9 μm, 115 fs, 1.7 mJ probe pulse. The residual OPCPA pump (1064 nm, 120 ps, <250 mJ) was split into two pump beams to drive a grating in one of two distinct target configurations: (1) a 2.5-mm-diameter carbon dioxide (CO_2) jet flowing into atmospheric air or (2) a 3.5-mm-diameter argon-cluster jet flowing into vacuum, as drawn in Fig. 1(d). The horizontally polarized pumps were focused a distance z_f from their crossing point in the jet. For the CO_2 configuration, the crossing half-angle was $\theta_0 = 1.2°$ with beam diameter 200 μm and $z_f = 8$ mm, and an example profile is shown in Fig. 1(c). For the cluster configuration, $\theta_0 = 2°$ with beam diameter 400 μm and $z_f = -23$ mm. These crossing angles correspond to grating periods (Λ) of 25 μm and 15 μm, respectively. The average grating density was measured using interferometry as between 3 and 8×10^{18} cm^{-3} in the CO_2 configuration and up to 1.5×10^{19} cm^{-3} in the cluster configuration. Argon clusters are van der Waals-bonded aggregates of argon atoms and have a reduced ionization threshold compared to atomic and molecular gases [56], allowing a higher plasma density to be produced with lower pump intensity. As a result, the pump beams were further from focus (larger z_f) in the cluster configuration and provided both a larger diameter (400 μm) grating and a higher plasma density (Supplement 1). The probe was focused to a 120 μm (in x) by 70 μm (in y) full-width-half-maximum (FWHM) spot. With up to 1.7 mJ in the probe, the maximum peak power was 14 GW, and the intensity inside the grating reached 2×10^{14} W/cm^2.

The key metric of a grating—the diffraction efficiency—was measured by imaging scattering of the diffracted and undiffracted probe beams from a Teflon screen using a mid-infrared camera [57]; Fig. 2 shows example near-field (with respect to the lens) beam profiles. Figures 2(a) and 2(b) show the CO_2 jet configuration with the pump beams off and on, respectively, and Figs. 2(c) and 2(d) show the cluster jet configuration. In each image the right spot ($\theta > 0$) is the undiffracted probe, and in Figs. 2(b) and 2(d) the left spot is the diffracted beam. The diffracted beam only appeared when an interference pattern was produced by the pump beams; for example, blocking a single pump beam suppressed all diffraction. The values of the extinction ratio (η_1/η_0), which describes the diffractive switching behavior of the grating, are far higher than those previously achieved with ionization gratings. In Fig. 2(b), $\eta_1/\eta_0 = 1.3$, putting this CO_2 jet grating in the depletion regime. The ring-shaped residual zeroth-order beam

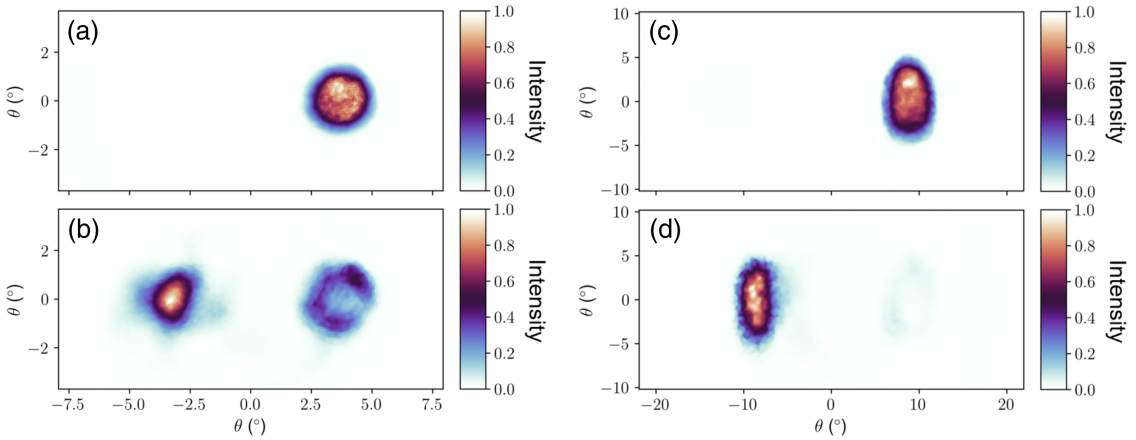

Fig. 2. Example probe beam profiles imaged on scattering screen. (a) Undiffracted probe (no jet or pump beams) and (b) diffracted (left) and residual zeroth order (right) beams in CO_2 jet configuration. (c) Undiffracted probe and (d) diffracted (left) and residual (right) beams in argon cluster jet configuration.

contains only 14% of the incident energy. However, in the CO_2 configuration, a substantial fraction of the incident energy was not transmitted at all, lowering the absolute diffraction efficiency ($\eta_1 = 0.18$) with $\eta_0 + \eta_1 = 0.32$ and an additional 10% of the incident energy arriving on the screen outside the η_0 and η_1 circles. Although absorption and scattering—the two likely sources of energy losses—reduce the total throughput efficiency and the immediate utility of this grating as an optic, they affect both the diffracted and undiffracted beams equally and can be analyzed separately from the diffraction process. Gratings formed from cluster jets [e.g., Fig. 2(d)] produced higher diffraction efficiency, with $\eta_1 = 0.60$ for Fig. 2(d); this improvement over the CO_2 grating can be attributed to both decreased losses ($\eta_1 + \eta_0 = 0.68$) and increased interaction strength ($\eta_1/\eta_0 = 8.7$). The weak residual zeroth order in this case also shows preferential depletion in its center. Little of the incident light (8%) makes it through the grating undiffracted.

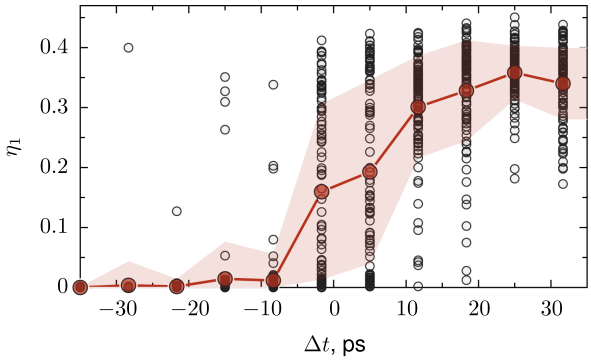

Fig. 3. First-order diffraction efficiency (η_1) as a function of the delay between the pump and probe pulses (argon cluster configuration). Black circles indicate individual single-shot measurements. Red circles show the mean efficiency at each delay. The shaded region marks the standard deviation of the efficiency over 100 shots.

B. Grating Dynamics

The dynamics of the grating formation were examined by varying the time delay between the pump pulses and the 3.9 μm probe (Δt). In Fig. 3, η_1 for a cluster jet ionization grating is plotted against Δt with both single-shot and average measurements marked. Although the average efficiency rises to $\eta_1 = 0.36$ over 35 ps, the bimodal distribution of single-shot measurements at $-5\ \text{ps} < \Delta t < 10\ \text{ps}$ suggests that the rise time of the grating itself is much faster; the slow increase in average efficiency is due to a change in the fraction of high-efficiency shots. The variation in turn-on time is likely the result of the high sensitivity of the avalanche-ionization delay time to pump intensity and neutral species density, which causes the plasma grating formation delay to fluctuate with these parameters. The presence of some high-efficiency shots at short delays is also consistent with turn-on time fluctuations. For $\Delta t > 25$ ps, the standard deviation of the efficiency drops to 0.05, showing that reasonable energy stability at high average efficiency is possible with this grating.

Similar behavior in time appears for gratings formed in CO_2. Figure 4 summarizes how the probe spatial quality [Fig. 4(a)] and extinction ratio η_1/η_0 [Fig. 4(b)] change with the probe delay at three different values of the combined pump energy. Unlike femtosecond-laser-driven gratings, which reach their maximum efficiency within a picosecond [42,51], the average diffraction efficiency observed in these avalanche-ionization gratings builds up over 10–100 ps, before decaying on a 100 ps timescale. The gratings form earlier for increased pump energy, in line with the intensity dependence of grating formation. We also find higher relative diffraction efficiency and higher absorption for the larger pump energies, which agrees with the observation that higher pump energies produce higher plasma density. Absorption increases in time: Figure 4(c) shows the decrease of the total transmitted probe energy ($\eta_0 + \eta_1$) for longer delays. Transmission did not rise for $\Delta t > 150$ ps, even as the extinction ratio falls, suggesting that the decrease of η_1/η_0 is a result of hydrodynamic expansion of the fringes reducing grating modulation rather than plasma recombination; this is consistent with our interferometry measurements, which likewise show no decrease in plasma density [57].

Expected values of absorption and the hydrodynamic timescale for the CO_2 configuration can be found by estimating the plasma electron temperature (T_e) from the collisional heating rate, $dT_e/dt \approx m_e(a_0 c)^2 \nu_{ei}/3$, where ν_{ei} is the electron-ion collision frequency and a_0 is the normalized vector potential [57]. From this, our plasma densities and pump intensities suggest

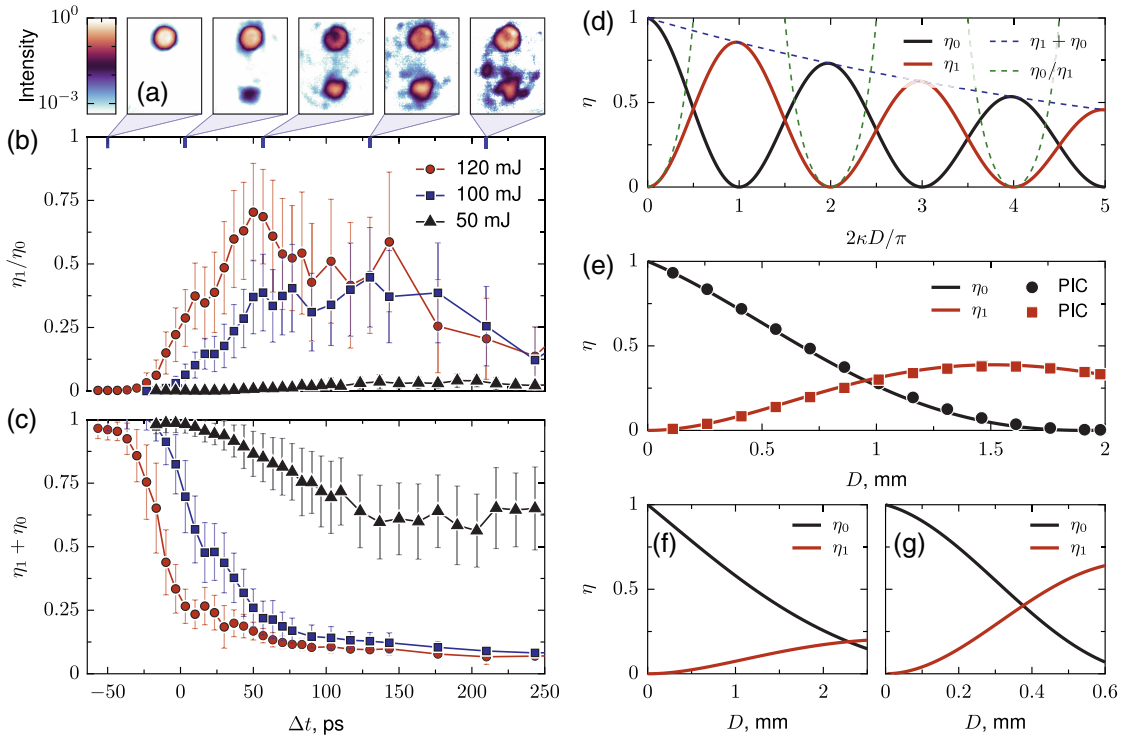

Fig. 4. Diffraction efficiency and absorption for ionization gratings (CO_2 configuration). (a) Undiffracted (upper) and diffracted (lower) probe spatial profiles at different delays (100 mJ pump energy) on a logarithmic intensity scale, showing decreasing beam quality at late times. (b) Extinction ratio (η_1/η_0) and (c) useful transmission ($\eta_1+\eta_0$) at varied probe time delay and total pump energies from 50 to 120 mJ. Each point is the mean of 200 shots, with the error bars marking the standard deviation. (d) First-order (η_1) and zeroth-order (η_0) efficiency, as well as their sum and ratio, according to Eq. (2) with $\kappa_c = \kappa/10$. (e) Analytic calculation and results from PIC simulation of diffraction from a grating with $N_{e,0} = 5.15 \times 10^{18}$ cm^{-3}, $N_{e,1} = 1.5 \times 10^{17}$ cm^{-3}, $T_e = 10$ eV, and varied thickness (D). (f) Analytic prediction for $N_{e,0} = 4.5 \times 10^{18}$ cm^{-3}, $N_{e,1} = 6.25 \times 10^{16}$ cm^{-3}, and $T_e = 10$ eV, which approximately reproduces efficiency shown in Fig. 2(b). (g) Analytic prediction for $N_{e,0} = 6 \times 10^{18}$ cm^{-3}, $N_{e,1} = 3.8 \times 10^{17}$ cm^{-3}, and $T_e = 12$ eV, which approximately reproduces efficiency shown in Fig. 2(d).

T_e in the range 5–30 eV, although this expression neglects heat conduction and may overestimate temperature. The hydrodynamic motion of ions occurs at the scale of the ion sound speed: $c_s = \sqrt{ZT_e/m_i}$, where m_i is the ion mass and Z is the ion charge number. We expect distortion on a timescale of order $0.1\Lambda/c_s$; for singly ionized CO_2, $T_e = 10$ eV, and $\Lambda = 10$ μm, this gives 200 ps, which is roughly consistent with the time over which the grating efficiency decreases. The spatial rate of absorption is $\kappa_c = (N_{e,0}/N_c)\nu_{ei}/c$, which for length D leads to an absorption fraction $A = \exp(-\kappa_c D)$ [57]. Since the zeroth-order and diffracted probe are entirely overlapped within the plasma grating, linear absorption acts on both identically, and the diffraction efficiency of a transmission grating with absorption is

$$\eta_1 = \sin^2(\kappa D) e^{-\kappa_c D}. \tag{2}$$

This, the complementary value for η_0, and the derived quantities η_1/η_0 and $\eta_1+\eta_0$ are plotted in Fig. 4(d) for $\kappa_c = \kappa/10$. In general, the relationship between the absorption length scale and the length required for complete diffraction (D_1) follows $\kappa_c D_1 \approx 2\pi(N_{e,0}/N_{e,1})(\nu_{ei}/\omega_1)\cos\theta_B$, where to minimize absorption we want $\kappa_c D_1 \ll 1$. In the results presented here, absorption does not prevent high diffraction efficiency, although it may be a limiting factor for gratings that are far from ideal ($N_{e,1} \ll N_{e,0}$); Fig. 4(e) shows that diffraction observed in a two-dimensional PIC simulation [57] of a grating closely follows Eq. (2). The separation of diffraction efficiency and absorption allows the density modulation and, assuming a temperature, the average plasma density to be estimated. In Figs. 4(f) and 4(g), analytic predictions for diffraction efficiency are plotted for parameters that produce the extinction ratio and absorption observed in Figs. 2(b) and 2(d), respectively. The average densities are within the bounds suggested by interferometry, and the temperatures are consistent with the above calculation.

In both the CO_2 and cluster configurations, the sinusoidal density modulation calculated from diffraction efficiency is much smaller than the maximum supported by the observed mean densities. The deviation from an ideal grating may arise from the non-sinusoidal shape of the density profile due to the nonlinearity of ionization, inhomogeneity of the pump profiles, hydrodynamic expansion of the plasma fringes, imperfect fringe contrast, and phase curvature of the pumps. The last point, due to using out-of-focus beams, introduces a subtle, but important, change to the grating structure. Since the local ray angle varies across the transverse width of the pump beams, the grating period varies in z as $\Lambda(z) = \Lambda_0(1 - z/z_f)$, reducing the effective length of the grating due to the changing Bragg angle and limited bandwidth. Choosing $D/z_f \ll 1$ minimizes this effect, a condition that the cluster configuration satisfies ($D/z_f \approx 0.02$), but the CO_2 configuration does not ($D/z_f \approx 0.3$).

C. Diffracted Beam Spatial Quality

In addition to reasonable efficiency, a useful plasma optic must not substantially degrade the spatial quality of the diffracted beam.

The high diffracted beam stability achieved here allowed measurement of the gratings' optical properties, including the spatial quality of the diffracted beams. For the CO_2 configuration, the probe focus achieved without the gas jet or pump beams [Fig. 5(a)] and that achieved for the diffracted beam [Fig. 5(b)] are almost indistinguishable in quality and size, showing that a plasma optic can efficiently redirect a beam while maintaining its focusability. Figure 5(c) shows that, as the probe delay increases, the peak intensity (I) in the focal spot rises to a maximum within 50 ps and then slowly decays. The standard deviations of the horizontal (σ_H) and vertical (σ_V) components of the centroid position fell between 50 μm and 100 μm for $\Delta t < 50$ ps. Although the beam pointing is less stable than that of the probe before the interaction (dashed lines, $\sigma_{H,0} = 8$ μm, $\sigma_{V,0} = 5$ μm), both σ_H and σ_V were less than half the spot FWHM. At later times, the peak intensity decreased, the horizontal motion of the spot increased, and the beam quality (see inset images) worsened, indicating a loss of quality of the grating fringes.

D. Damage Threshold Measurements

To characterize the performance of the ionization gratings at high probe power and intensity, we measured η_1 for increasing probe energy in a cluster grating (Fig. 6). The average efficiency decreased above 0.3 mJ, suggesting a threshold for linear probe propagation through the grating. With 210 mJ in the driving pumps and a probe spot size of 5% of the grating transverse area, this corresponds to a peak incident probe intensity about 30 times the peak pump intensity and a peak probe power about 1.5 times that of the pumps. However, it is important to note that single-shot

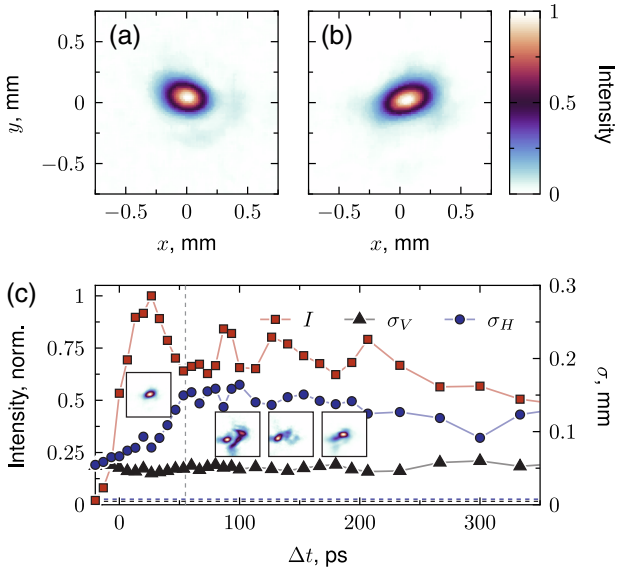

Fig. 5. Far field probe quality (CO_2 configuration). (a) Focal spot of probe without jet or pumps. (b) Focal spot of the first-order diffracted beam. (c) Variation of the peak diffracted focal spot intensity (I, red squares) and the standard deviation of the vertical (σ_V, black triangles) and horizontal (σ_H, blue circles) focal spot centroid positions against the probe delay time. Each point represents the average (intensity) or standard deviation (position) of a set of 500 individual shots. Inset images are characteristic examples of the diffracted beam focal spot at different time delays. The vertical dashed line marks the transition between the relatively stable, high-spot-quality regime at short delays and the less stable regime at longer delays. The horizontal dashed lines show σ_H and σ_V of the zeroth-order beam without the gas jet.

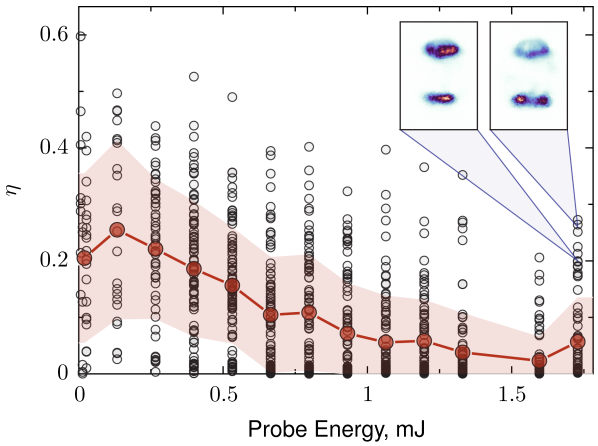

Fig. 6. First-order diffraction efficiency (η_1) as a function of the probe pulse energy (argon cluster configuration). Black circles indicate individual single-shot measurements. Red circles show the mean efficiency (over 100 shots) at each delay. The shaded region marks the standard deviation of the efficiency. Inset images show the undiffracted (upper) and diffracted (lower) beam profiles at two 1.7 mJ points.

efficiencies above 0.2 were observed at all tested values of the probe energy. Although a fraction of these high-energy high-efficiency measurements correspond to diffracted beams with poor spatial quality, including the characteristic dual-peak structure shown in the right inset of Fig. 6, others correspond to high-spatial-quality diffraction, like that shown in the left inset. Some of the produced gratings, therefore, efficiently diffracted a probe with intensity 1.7×10^{14} W/cm^2, more than 170 times the pump intensity, suggesting that if the process can be scaled to larger area, higher probe power could be controlled. Shot-to-shot variations in probe energy were less than 2% and, therefore, cannot account for the large variations in diffraction efficiency, which are likely a result of shot-to-shot fluctuations in grating density and shape. The grating formation is sensitive to the pump intensity, so the fluctuations of pump intensity produce gratings with a relatively wide range of sizes and densities; some combinations of these parameters appear to be exceptionally efficient and robust to probe intensity. Though the variability limits the immediate usefulness of these gratings, the observation of high single-shot efficiencies at high probe intensity suggests that, with improved beam stability and understanding of the parameters that produce high performance, substantial increases in average efficiency are possible.

3. DISCUSSION

To be deployed, plasma optics must operate with reasonable efficiency (e.g., >50%) and stability at a substantially higher damage threshold than a solid-state equivalent, be able to manipulate more power or energy in the probe than was required to create the optic, and not degrade the spatial or temporal quality of the beam. We have shown here that we are not limited to the low efficiencies of previously demonstrated plasma gratings. Average efficiencies in these experiments of up to 36% are far higher than previous results and near what is required for a practical optic, and individual measurements exceed 50%, demonstrating that, with the right laser and plasma parameters, it is possible to construct a high-efficiency grating. Both the focusability and the pointing stability of the diffracted beam also appear to be sufficient for future applications, and we have shown that high-performance persists at probe beam

intensities that would destroy solid-state materials. Furthermore, the intensity in the manipulated probe can exceed that of the pumps that were used to create the grating.

Although these results represent a proof-of-principle demonstration of an ionization grating operating in a high-efficiency regime, substantial work is needed to make these optics a reality, from determining the most efficient mechanisms for forming a grating to adequately stabilizing grating output. This study has several limitations that future work would need to address before an ionization grating could be used as a component in a high-power beamline. First, the highest efficiencies were reached for only a small subset of interactions. Although promising, in that even a single measurement of efficient diffraction shows that high efficiency is possible, a useful optic would need to reach these efficiencies on almost all interactions. Detailed study of grating properties and optimization of laser and plasma parameters would be needed to both determine the key differences for high-efficiency interactions and then reproduce them reliably. Second, although we show that interactions at high probe intensity can still be efficient, we see an efficiency decrease at higher probe energies. Alternate target materials may provide a more robust grating at the cost of more difficult grating formation, but significant work on the ideal method for forming a grating must still be done. Third, the total energy in our probe beam is still relatively low, limited in part by the pump and probe capabilities of the laser system that we used to run this experiment. Scaling the diameter of a grating to a larger size to allow higher probe energy will eventually be necessary. And finally, to make this initial demonstration, we have taken advantage of the lower density requirement of 3.9 μm light for efficient diffraction compared to $\lambda_1 = 800$ or 1000 nm, where most high-power lasers operate. The plasma critical density scales with inverse wavelength squared, and the required grating length is proportional to wavelength, so achieving equivalent performance at 800 nm for this grating size requires a fivefold increase in plasma density or a corresponding improvement of grating quality. Both are plausible routes to a high-performance plasma optic suitable for near-infrared light and, ultimately, high-power plasma-based lasers.

These experiments show that ionization gratings can meet the key requirements of a plasma optic and could form the basis of high-flux diffractive lenses or compact ultra-high-power lasers based on a plasma transmission grating design [13]. In particular, we report dramatically higher average and single-shot diffraction efficiency from an ionization grating than previously demonstrated and for the first time create an ionization transmission grating. This work also reports the first measurements of the focusability and spatial quality of a beam diffracted from an ionization grating. These results were in part enabled by taking a new, avalanche-ionization-based approach to grating formation, indicating that avalanche ionization is a promising alternative to field ionization for the creation of ionization optics. Taken together, these results suggest that ionization volume gratings are a viable path toward using plasma optics as the basis for the next generation of high-power lasers.

Funding. Lawrence Livermore National Laboratory (20-ERD-057, 21-LW-013); National Science Foundation (PHY2010511); Air Force Office of Scientific Research (FA9550-16-1-0259, FA9550-16-1-0284).

Acknowledgment. Lawrence Livermore National Laboratory is operated by Lawrence Livermore National Security, LLC, for the U.S. Department of Energy, National Nuclear Security Administration. The authors thank R. Schwartz for assistance with experiments.

Disclosures. The authors declare no conflicts of interest.

Data availability. Data underlying the results presented in this paper are not publicly available at this time but may be obtained from the authors upon reasonable request.

Supplemental document. See Supplement 1 for supporting content.

REFERENCES

1. E. Cartlidge, "The light fantastic," Science **359**, 382–385 (2018).
2. G. A. Mourou, T. Tajima, and S. V. Bulanov, "Optics in the relativistic regime," Rev. Mod. Phys. **78**, 309–371 (2006).
3. C. Geddes, C. Toth, J. Van Tilborg, E. Esarey, C. Schroeder, D. Bruhwiler, C. Nieter, J. Cary, and W. Leemans, "High-quality electron beams from a laser wakefield accelerator using plasma-channel guiding," Nature **431**, 538–541 (2004).
4. E. Esarey, C. Schroeder, and W. Leemans, "Physics of laser-driven plasma-based electron accelerators," Rev. Mod. Phys. **81**, 1229–1285 (2009).
5. A. Macchi, M. Borghesi, and M. Passoni, "Ion acceleration by superintense laser-plasma interaction," Rev. Mod. Phys. **85**, 751–793 (2013).
6. H. Chen, F. Fiuza, A. Link, A. Hazi, M. Hill, D. Hoarty, S. James, S. Kerr, D. D. Meyerhofer, J. Myatt, J. Park, Y. Sentoku, and G. J. Williams, "Scaling the yield of laser-driven electron-positron jets to laboratory astrophysical applications," Phys. Rev. Lett. **114**, 215001 (2015).
7. S. Meuren, P. H. Bucksbaum, N. J. Fisch, F. Fiúza, S. Glenzer, M. J. Hogan, K. Qu, D. A. Reis, G. White, and V. Yakimenko, "On seminal HEDP research opportunities enabled by colocating multi-petawatt laser with high-density electron beams," arXiv, arXiv:2002.10051 (2020).
8. S. Weber, S. Bechet, S. Borneis, *et al.*, "P3: an installation for high-energy density plasma physics and ultra-high intensity laser–matter interaction at ELI-Beamlines," Matter Radiat. Extremes **2**, 149–176 (2017).
9. D. Strickland and G. Mourou, "Compression of amplified chirped optical pulses," Opt. Commun. **55**, 447–449 (1985).
10. J. Schwinger, "On gauge invariance and vacuum polarization," Phys. Rev. **82**, 664–679 (1951).
11. A. Di Piazza, C. Müller, K. Hatsagortsyan, and C. Keitel, "Extremely high-intensity laser interactions with fundamental quantum systems," Rev. Mod. Phys. **84**, 1177–1228 (2012).
12. H. Milchberg, "Indestructible plasma optics," Phys. Today **72**(6), 70–71 (2019).
13. M. R. Edwards and P. Michel, "Plasma transmission gratings for compression of high-intensity laser pulses," Phys. Rev. Appl. **18**, 024026 (2022).
14. V. M. Malkin, G. Shvets, and N. J. Fisch, "Fast compression of laser beams to highly overcritical powers," Phys. Rev. Lett. **82**, 4448–4451 (1999).
15. Y. Ping, W. Cheng, S. Suckewer, D. S. Clark, and N. J. Fisch, "Amplification of ultrashort laser pulses by a resonant Raman scheme in a gas-jet plasma," Phys. Rev. Lett. **92**, 175007 (2004).
16. A. Andreev, C. Riconda, V. Tikhonchuk, and S. Weber, "Short light pulse amplification and compression by stimulated Brillouin scattering in plasmas in the strong coupling regime," Phys. Plasmas **13**, 053110 (2006).
17. R. Trines, F. Fiuza, R. Bingham, R. Fonseca, L. Silva, R. Cairns, and P. Norreys, "Simulations of efficient Raman amplification into the multipetawatt regime," Nat. Phys. **7**, 87–92 (2011).
18. G. Lehmann and K. Spatschek, "Nonlinear Brillouin amplification of finite-duration seeds in the strong coupling regime," Phys. Plasmas **20**, 073112 (2013).
19. M. R. Edwards, Q. Jia, J. M. Mikhailova, and N. J. Fisch, "Short-pulse amplification by strongly-coupled stimulated Brillouin scattering," Phys. Plasmas **23**, 083122 (2016).
20. D. Turnbull, S. Bucht, A. Davies, D. Haberberger, T. Kessler, J. Shaw, and D. Froula, "Raman amplification with a flying focus," Phys. Rev. Lett. **120**, 024801 (2018).
21. J.-R. Marquès, L. Lancia, T. Gangolf, M. Blecher, S. Bolaños, J. Fuchs, O. Willi, F. Amiranoff, R. Berger, M. Chiaramello, and S. Weber, "Joule-level high-efficiency energy transfer to subpicosecond laser pulses by a plasma-based amplifier," Phys. Rev. X **9**, 021008 (2019).
22. P. Michel, L. Divol, D. Turnbull, and J. Moody, "Dynamic control of the polarization of intense laser beams via optical wave mixing in plasmas," Phys. Rev. Lett. **113**, 205001 (2014).

23. K. Qu, Q. Jia, and N. J. Fisch, "Plasma q-plate for generation and manipulation of intense optical vortices," Phys. Rev. E **96**, 053207 (2017).
24. D. Turnbull, C. Goyon, G. Kemp, B. Pollock, D. Mariscal, L. Divol, J. Ross, S. Patankar, J. Moody, and P. Michel, "Refractive index seen by a probe beam interacting with a laser-plasma system," Phys. Rev. Lett. **118**, 015001 (2017).
25. J. P. Palastro, D. Gordon, B. Hafizi, L. A. Johnson, J. Peñano, R. F. Hubbard, M. Helle, and D. Kaganovich, "Plasma lenses for ultrashort multi-petawatt laser pulses," Phys. Plasmas **22**, 123101 (2015).
26. G. Lehmann and K. Spatschek, "Plasma volume holograms for focusing and mode conversion of ultraintense laser pulses," Phys. Rev. E **100**, 033205 (2019).
27. M. R. Edwards, V. R. Munirov, A. Singh, N. Fasano, E. Kur, N. Lemos, J. M. Mikhailova, J. S. Wurtele, and P. Michel, "Holographic plasma lenses," Phys. Rev. Lett. **128**, 065003 (2022).
28. N. Lemos, L. Cardoso, J. Geada, G. Figueira, F. Albert, and J. Dias, "Guiding of laser pulses in plasma waveguides created by linearly-polarized femtosecond laser pulses," Sci. Rep. **8**, 3165 (2018).
29. B. Miao, L. Feder, J. E. Shrock, A. Goffin, and H. M. Milchberg, "Optical guiding in meter-scale plasma waveguides," Phys. Rev. Lett. **125**, 074801 (2020).
30. C. Thaury, F. Quéré, J.-P. Geindre, A. Levy, T. Ceccotti, P. Monot, M. Bougeard, F. Réau, P. d'Oliveira, P. Audebert, R. Marjoribanks, and P. Martin, "Plasma mirrors for ultrahigh-intensity optics," Nat. Phys. **3**, 424–429 (2007).
31. J. M. Mikhailova, A. Buck, A. Borot, K. Schmid, C. Sears, G. D. Tsakiris, F. Krausz, and L. Veisz, "Ultra-high-contrast few-cycle pulses for multipetawatt-class laser technology," Opt. Lett. **36**, 3145–3147 (2011).
32. M. R. Edwards, N. M. Fasano, T. Bennett, A. Griffith, N. Turley, B. M. O'Brien, and J. M. Mikhailova, "A multi-terawatt two-color beam for high-power field-controlled nonlinear optics," Opt. Lett. **45**, 6542–6545 (2020).
33. M. R. Edwards and J. M. Mikhailova, "The x-ray emission effectiveness of plasma mirrors: reexamining power-law scaling for relativistic high-order harmonic generation," Sci. Rep. **10**, 5154 (2020).
34. S. Suntsov, D. Abdollahpour, D. Papazoglou, and S. Tzortzakis, "Femtosecond laser induced plasma diffraction gratings in air as photonic devices for high intensity laser applications," Appl. Phys. Lett. **94**, 251104 (2009).
35. G. Lehmann and K. H. Spatschek, "Transient plasma photonic crystals for high-power lasers," Phys. Rev. Lett. **116**, 225002 (2016).
36. H. Peng, C. Riconda, M. Grech, J.-Q. Su, and S. Weber, "Nonlinear dynamics of laser-generated ion-plasma gratings: a unified description," Phys. Rev. E **100**, 061201 (2019).
37. F. Lureau, G. Matras, O. Chalus, *et al.*, "High-energy hybrid femtosecond laser system demonstrating 2×10 PW capability," High Power Laser Sci. Eng. **8**, e43 (2020).
38. T. Wittmann, J.-P. Geindre, P. Audebert, R. Marjoribanks, J.-P. Rousseau, F. Burgy, D. Douillet, T. Lefrou, K. T. Phuoc, and J.-P. Chambaret, "Towards ultrahigh-contrast ultraintense laser pulses-complete characterization of a double plasma-mirror pulse cleaner," Rev. Sci. Instrum. **77**, 083109 (2006).
39. A. Lévy, T. Ceccotti, P. D'Oliveira, F. Réau, M. Perdrix, F. Quéré, P. Monot, M. Bougeard, H. Lagadec, P. Martin, J.-P. Geindre, and P. Audebert, "Double plasma mirror for ultrahigh temporal contrast ultraintense laser pulses," Opt. Lett. **32**, 310–312 (2007).
40. I. Kim, I. Choi, S. Lee, K. Janulewicz, J. Sung, T. Yu, H. Kim, H. Yun, T. Jeong, and J. Lee, "Spatio-temporal characterization of double plasma mirror for ultrahigh contrast and stable laser pulse," Appl. Phys. B **104**, 81–86 (2011).
41. X. Yang, J. Wu, Y. Tong, L. Ding, Z. Xu, and H. Zeng, "Femtosecond laser pulse energy transfer induced by plasma grating due to filament interaction in air," Appl. Phys. Lett. **97**, 071108 (2010).
42. L. Shi, W. Li, Y. Wang, X. Lu, and H. Zeng, "Generation of high-density electrons based on plasma grating induced Bragg diffraction in air," Phys. Rev. Lett. **107**, 095004 (2011).
43. J. Liu, W. Li, H. Pan, and H. Zeng, "Two-dimensional plasma grating by non-collinear femtosecond filament interaction in air," Appl. Phys. Lett. **99**, 151105 (2011).
44. M. Durand, Y. Liu, B. Forestier, A. Houard, and A. Mysyrowicz, "Experimental observation of a traveling plasma grating formed by two crossing filaments in gases," Appl. Phys. Lett. **98**, 121110 (2011).
45. J. K. Wahlstrand and H. M. Milchberg, "Effect of a plasma grating on pump–probe experiments near the ionization threshold in gases," Opt. Lett. **36**, 3822–3824 (2011).
46. M. Durand, A. Jarnac, Y. Liu, B. Prade, A. Houard, V. Tikhonchuk, and A. Mysyrowicz, "Dynamics of plasma gratings in atomic and molecular gases," Phys. Rev. E **86**, 036405 (2012).
47. J. K. Wahlstrand, J. H. Odhner, E. T. McCole, Y.-H. Cheng, J. P. Palastro, R. J. Levis, and H. M. Milchberg, "Effect of two-beam coupling in strong-field optical pump-probe experiments," Phys. Rev. A **87**, 053801 (2013).
48. Z.-M. Sheng, J. Zhang, and D. Umstadter, "Plasma density gratings induced by intersecting laser pulses in underdense plasmas," Appl. Phys. B **77**, 673–680 (2003).
49. P. Zhang, N. Saleh, S. Chen, Z. Sheng, and D. Umstadter, "Laser-energy transfer and enhancement of plasma waves and electron beams by interfering high-intensity laser pulses," Phys. Rev. Lett. **91**, 225001 (2003).
50. L. Friedland, G. Marcus, J. Wurtele, and P. Michel, "Excitation and control of large amplitude standing ion acoustic waves," Phys. Plasmas **26**, 092109 (2019).
51. M. R. Edwards, N. M. Fasano, N. Lemos, A. Singh, V. Munirov, E. Kur, J. S. Wurtele, J. M. Mikhailova, and P. Michel, "Measuring the optical properties of ionization gratings in air for control of femtosecond lasers," in *CLEO: Fundamental Science* (2021).
52. A. Couairon and A. Mysyrowicz, "Femtosecond filamentation in transparent media," Phys. Rep. **441**, 47–189 (2007).
53. D. Woodbury, R. Schwartz, E. Rockafellow, J. K. Wahlstrand, and H. Milchberg, "Absolute measurement of laser ionization yield in atmospheric pressure range gases over 14 decades," Phys. Rev. Lett. **124**, 013201 (2020).
54. P. Yeh, *Introduction to Photorefractive Nonlinear Optics*, Wiley Series in Pure and Applied Optics (Wiley, 1993).
55. R. W. Boyd, *Nonlinear Optics*, 3rd ed. (Academic, 2008).
56. H. Sheng, K. Kim, V. Kumarappan, B. Layer, and H. Milchberg, "Plasma waveguides efficiently generated by Bessel beams in elongated cluster gas jets," Phys. Rev. E **72**, 036411 (2005).
57. P. Michel, *Introduction to Laser-Plasma Interactions* (Springer, 2022).